Article

# In Situ Quantum Dot Growth on Multiwalled Carbon Nanotubes

Sarbajit Banerjee, and Stanislaus S. Wong

*J. Am. Chem. Soc.*, **2003**, 125 (34), 10342-10350• DOI: 10.1021/ja035980c • Publication Date (Web): 31 July 2003

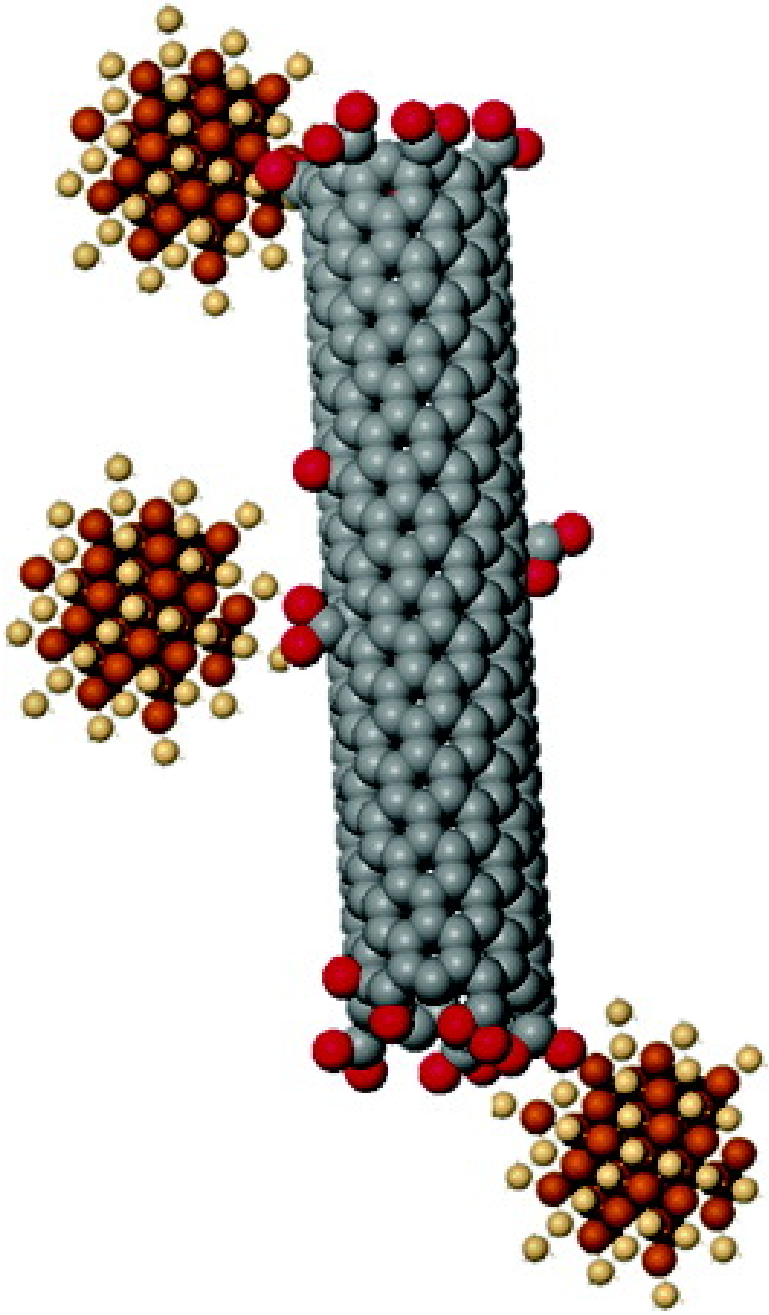

## More About This Article

Additional resources and features associated with this article are available within the HTML version:

J|A|C|S
ARTICLES
Published on Web 07/31/2003

# In Situ Quantum Dot Growth on Multiwalled Carbon Nanotubes

Sarbajit Banerjee[†] and Stanislaus S. Wong*[,†,§]

*Contribution from the Department of Chemistry, State University of New York at Stony Brook, Stony Brook, New York 11794-3400, and the Materials and Chemical Sciences Department, Brookhaven National Laboratory, Building 480, Upton, New York 11973*

Received May 6, 2003; E-mail: sswong@notes.cc.sunysb.edu; sswong@bnl.gov

***Abstract:*** The generation of nanoscale interconnects and supramolecular, hierarchical assemblies enables the development of a number of novel nanoscale applications. A rational approach toward engineering a robust system is through chemical recognition. Here, we show the in situ mineralization of crystalline CdTe quantum dots on the surfaces of oxidized multiwalled carbon nanotubes (MWNTs). We coordinate metallic precursors of quantum dots directly onto nanotubes and then proceed with in situ growth. The resulting network of molecular-scale "fused" nanotube−nanocrystal heterojunctions demonstrates a controlled synthetic route to the synthesis of complex nanoscale heterostructures. Extensive characterization of these heterostructures has been performed using scanning electron microscopy (SEM), transmission electron microscopy (TEM), high-resolution transmission electron microscopy (HRTEM), energy-dispersive X-ray spectroscopy (EDS), X-ray photoelectron spectroscopy (XPS), Raman spectroscopy, UV−visible spectroscopy, and X-ray diffraction (XRD).

## Introduction

Carbon nanotubes (CNTs) have unique structural, electronic, mechanical, and optical properties, with applications in many fields.[1] CNTs need to be controllably assembled into various designed architectures, a key to building complex, functional nanotube devices. In other words, CNTs need to be arranged into well-defined configurations in order to design integrated systems. Although nanostructure assembly motifs can be based on biological recognition or through lithography,[2,3] the construction of supramolecular hierarchical assemblies[4] made of CNTs is one task in which the fundamental understanding and application of nanotube chemistry can play a central role. This work takes advantage of our use of nanotubes as coordination ligands to rationally construct nanotube-based composites. Thus, the approach proposed herein differs from previous attempts to synthesize nanotube assemblies in that we use in situ growth processes to control the placement of our nanocomponents. Work in the past has focused on generating nanotube networks, using either a nanotube suspension or a modified chemical vapor deposition procedure,[5,6] onto solid, prepatterned substrates.[7−9] The resulting nanocomposite materials would be expected to be important for applications ranging from high-efficiency computing, high-density data storage media, light harvesting in photovoltaic cells, lightweight, high-strength textiles, to supersensitive sensors and drug delivery agents.[10−12]

Chemical modification strategies have generally targeted CNT defects, end caps, sidewalls, as well as the hollow interior.[13−15] Representative approaches to CNT derivatization include covalent chemistry of conjugated double bonds within the nanotube,[16−18] noncovalent $\pi$-stacking,[19] covalent interactions at dangling functionalities at nanotube ends and defects,[20] and wrapping of macromolecules.[21−23] In addition, nanotube-based heterostructures have been chemically synthesized on the basis

† State University of New York at Stony Brook.
§ Brookhaven National Laboratory.

(1) Dresselhaus, M. S.; Dresselhaus, G.; Avouris, P. *Carbon Nanotubes: Synthesis, Structure, Properties, and Applications*; Springer-Verlag: New York, 2001.
(2) Mitchell, G. P.; Mirkin, C. A.; Letsinger, R. L. *J. Am. Chem. Soc.* **1999**, *121*, 8122.
(3) Yang, Y.; Huang, S.; He, H.; Mau, A. W. H.; Dai, L. *J. Am. Chem. Soc.* **1999**, *121*, 10832.
(4) Sano, M.; Kamino, A.; Okamura, J.; Shinkai, S. *Nano Lett.* **2002**, *2*, 531.
(5) Cassell, A. M.; McCool, G. C.; Ng, H. T.; Koehne, J. E.; Chen, B.; Li, J.; Han, J.; Meyyappan, M. *Appl. Phys. Lett.* **2003**, *82*, 817.
(6) Zhang, Z.; Wei, B.; Ajayan, P. M. *Chem. Commun.* **2002**, *9*, 962.
(7) Choi, K. H.; Bourgoin, J. P.; Auvray, S.; Esteve, D.; Duesberg, G. S.; Roth, S.; Burghard, M. *Surf. Sci.* **2000**, *462*, 195.
(8) Lewenstein, J. C.; Burgin, T. P.; Ribayroi, A.; Nagahara, L. A.; Tsui, R. K. *Nano Lett.* **2002**, *2*, 443.
(9) Wei, B. Q.; Vajtai, R.; Jung, Y.; Ward, J.; Zhang, R.; Ramanath, G.; Ajayan, P. M. *Nature* **2002**, *416*, 495.
(10) Avouris, P. *Acc. Chem. Res.* **2002**, *35*, 1026.
(11) Huynh, W. U.; Dittmer, J. J.; Alivisatos, A. P. *Science* **2002**, *295*, 2425.
(12) Kong, J.; Franklin, N. R.; Zhou, C.; Chapline, M. G.; Peng, S.; Cho, K.; Dai, H. *Science* **2000**, *287*, 622.
(13) Hirsch, A. *Angew. Chem., Int. Ed.* **2002**, *41*, 1853. Banerjee, S.; Kahn, M. G. C.; Wong, S. S. *Chem. Eur. J.* **2003**, *9*, 1898.
(14) Sinnott, S. B. *J. Nanosci. Nanotechnol.* **2002**, *2*, 113.
(15) Bahr, J.; Tour, J. M. *J. Mater. Chem.* **2002**, *12*, 195.
(16) Bahr, J. L.; Yang, J.; Kosynkin, D. V.; Broniskowski, M. J.; Smalley, R. E.; Tour, J. M. *J. Am. Chem. Soc.* **2001**, *123*, 6536.
(17) Georgakilas, V.; Kordatos, K.; Prato, M.; Guldi, D. M.; Holzinger, M.; Hirsch, A. *J. Am. Chem. Soc.* **2002**, *124*, 760.
(18) Mickelson, E. T.; Huffman, C. B.; Rinzler, A. G.; Smalley, R. E.; Hauge, R. H.; Margrave, J. L. *Chem. Phys. Lett.* **1998**, *296*, 188.
(19) Chen, R. J.; Zhang, Y.; Wang, D.; Dai, H. *J. Am. Chem. Soc.* **2001**, *123*, 3838.
(20) Chen, J.; Hamon, M. A.; Hu, H.; Chen, Y.; Rao, A. M.; Eklund, P. C.; Haddon, R. C. *Science* **1998**, *282*, 95.
(21) O'Connell, M.; Boul, P.; Ericson, L. M.; Huffman, C.; Wang, Y.; Haroz, E.; Kuper, C.; Tour, J.; Ausman, K. D.; Smalley, R. E. *Chem. Phys. Lett.* **2001**, *342*, 265.
(22) Riggs, J. E.; Guo, Z.; Carroll, D. L.; Sun, Y.-P. *J. Am. Chem. Soc.* **2000**, *122*, 5879.


**10.1021/ja035980c CCC: $25.00** 

of a number of different strategies. These have included the coaxial growth of BN species around the nanotubes,[24,25] the controlled solid-state reaction involving nanorods or particles of silicon carbide and transition metal carbides,[26] and the catalytic growth of Si nanowires onto the ends of nanotubes.[27]

In our laboratory, oxidized CNTs have been reacted with cadmium selenide (CdSe) nanocrystals, capped with functionalized thiol derivatives as well as titanium dioxide ($TiO_2$) nanocrystals, functionalized with 11-aminoundecanoic acid to form quantum dot−nanotube heterostructures characterized by transmission electron microscopy and infrared spectroscopy. The resulting composite structure with acid-terminated CdSe nanocrystals and acid-terminated tubes was facilitated by an amide-forming reaction in the presence of 1-ethyl-3-(3-dimethylaminopropyl) carbodiimide hydrochloride, EDC.[28] Other groups have generated analogous systems using an essentially identical strategy with minor variations.[29−31] One of the limitations of this methodology is that it yields primarily unorganized, discrete one-dimensional "ball-and-stick" structures, which are very difficult to organize into an ordered assembly.

Herein, we show an in situ growth of CdTe nanocrystals on the surfaces of multiwalled carbon nanotubes (MWNTs). In principle, this involves the use of metal coordination to oxygenated, surface functional groups on MWNTs, which then act as specific nucleation sites for the growth of nanotube−nanocrystal interconnects. As examples of nanotube chemistry involving metal coordination, in previous work, we have derivatized SWNTs with relatively bulky inorganic complexes,[32,33] which not only yields a novel metal-based molecular coordination complex but also offers the possibility of tailorable solubility in a variety of solvents. In addition, these generated adducts can be used in a number of different catalytic processes, including homogeneous catalysis, upon which the expensive metal-support assembly can be facilely recovered from solution.[33] As another example of the versatility of metal complexation, MWNTs, functionalized with a ruthenium complex, have been utilized to create interconnects showing multiple T- and Y-junctions.[34]

In this work, MWNTs are being considered as sterically bulky, $\pi$-conjugated ligands and as crystal growth terminators in the in situ synthesis of CdTe nanocrystals, leading to the generation of tube-capped quantum dots. Its significance is that nanocrystals (demonstrated for CdTe) can then grow across the gap between tubes, forming a junction. Generating a junction incorporating both of these nanostructures is significant because it takes advantage of the tunability, in terms of size, shape, and chemistry, of nanotubes and nanocrystals, to create a sharp junction interface. These heterostructures will allow for an understanding of factors affecting carrier mobility in nanomaterials, such as electronic structure, carrier trapping, and delocalization, useful in the optimization of photovoltaic devices.[11] This is expected to lead to better charge separation and therefore more efficient light harvesting. One of the challenges of nanoscale heterostructure synthesis has been to chemically incorporate nanotubes into advanced composites, while at the same time, preserving favorable structural, electrical, optical, and mechanical properties for the resulting nanocomposite.[13−15]

The mineralization of CdTe on the nanotube surface should be generalizable for many other binary and more complex systems. Insights into crystal growth, specifically into oriented attachment at specific sites on nanotube surfaces, can also be obtained from these data. These MWNT−nanocrystal heterostructures have been structurally characterized by scanning electron microscopy (SEM), transmission electron microscopy (TEM), high-resolution transmission electron microscopy (HR-TEM), energy-dispersive X-ray spectroscopy (EDS), X-ray photoelectron spectroscopy (XPS), infrared spectroscopy, Raman spectroscopy, UV−visible spectroscopy, and X-ray diffraction (XRD).

## Experimental Section

**Nanotube Processing and Heterostructure Synthesis.** Multiwalled nanotubes (MWNTs) were obtained from MER Corporation. An aggressive functionalization protocol was used to remove almost all of the metal impurities (such as iron) and a substantial portion of the amorphous carbon entities in the sample.[35] In essence, a vigorous $KMnO_4/H_2SO_4$ treatment[35] was followed by successive processing with solutions of 35% HCl and 10% HF. The purified tubes were then extensively washed with distilled water and heated at 150 °C in a drying oven. XPS analysis, coupled with EDS data, have indicated that any remaining metal was below detectable limits.

This rigorous functionalization protocol opens and derivatizes most of the nanotube ends as well as attacks occasional defect sites[13] at the sidewalls. The generated functional groups are expected to be a mixture of carboxylic acids, alcohols, and ketones.[35] These functionalized, oxygenated nanotubes were used as ligands and as templates to grow CdTe nanocrystals. In a modification of a procedure developed by Peng et al. to synthesize high-quality CdTe nanocrystals using a one-pot approach with CdO,[36,37] MWNTs were mixed with CdO and tetradecylphosphonic acid (TDPA) and then were heated to 320 °C in trioctylphosphine oxide (TOPO) under argon with vigorous stirring. A substoichiometric amount of TDPA was used so that some of the Cd could coordinate to the oxygenated functional groups (especially carboxylic acid and alcohol groups) localized on the MWNT surface.

A Te solution in trioctylphosphine (TOP) was then injected at 300 °C, and the crystals were allowed to grow at 250 °C. After a 20 min growth period, the heating source was removed. Upon cooling to 50 °C, 5 mL of toluene was added to the reaction mixture, and nanocrystals were recovered through precipitation initiated by addition of methanol. The solid residue, which included functionalized tubes as well as CdTe nanocrystals not attached to the tubes, was filtered over a 0.2 $\mu$m PTFE membrane. CdTe nanocrystals, not bound to the tubes, were washed away by using copious amounts of toluene. Only functionalized heterostructures were retained on the membrane, and these were dried and used for further characterization.

(23) Star, A.; Stoddart, J. F.; Steurman, D.; Diehl, M.; Boukai, A.; Wong, E. W.; Yang, X.; Chung, S.-W.; Choi, H.; Heath, J. R. *Angew. Chem., Int. Ed.* **2001**, *40*, 1721.
(24) Zhang, Y.; Suenaga, K.; Colliex, C.; Iijima, S. *Science* **1998**, *281*, 973.
(25) Suenaga, K.; Colliex, C.; Demoncy, N.; Loiseau, A.; Pascard, H.; Willaime, F. *Science* **1997**, *278*, 653.
(26) Zhang, Y.; Ichihashi, T.; Landree, E.; Nihey, F.; Iijima, S. *Science* **1999**, *285*, 1719.
(27) Hu, J.; Ouyang, M.; Yang, P.; Lieber, C. M. *Nature* **1999**, *399*, 48.
(28) Banerjee, S.; Wong, S. S. *Nano Lett.* **2002**, *2*, 195.
(29) Ravindran, S.; Chaudhary, S.; Colburn, B.; Ozkan, M.; Ozkan, C. S. *Nano Lett.* **2003**, *3*, 447.
(30) Haremza, J. M.; Hahn, M. A.; Krauss, T. D.; Chen, S.; Calcines, J. *Nano Lett.* **2002**, *2*, 1253.
(31) Azamian, R.; Coleman, K.; Davis, J.; Hanson, N.; Green, M. *Chem. Commun.* **2002**, 366.
(32) Banerjee, S.; Wong, S. S. *Nano Lett.* **2002**, *2*, 49.
(33) Banerjee, S.; Wong, S. S. *J. Am. Chem. Soc.* **2002**, *124*, 8940.
(34) Frehill, F.; Vos, J. G.; Benrezzak, S.; Koos, A. A.; Konya, Z.; Ruther, M. G.; Blau, W. J.; Fonseca, A.; Nagy, J. B.; Biro, L. P.; Minett, A. I.; in Het Panhuis, M. *J. Am. Chem. Soc.* **2002**, *124*, 13694.
(35) Hiura, H.; Ebbesen, T. W.; Tanigaki, K. *Adv. Mater. (Weinheim, Ger.)* **1995**, *7*, 275.
(36) Peng, Z. A.; Peng, X. *J. Am. Chem. Soc.* **2001**, *123*, 183.
(37) Peng, Z. A.; Peng, X. *J. Am. Chem. Soc.* **2002**, *124*, 3343.

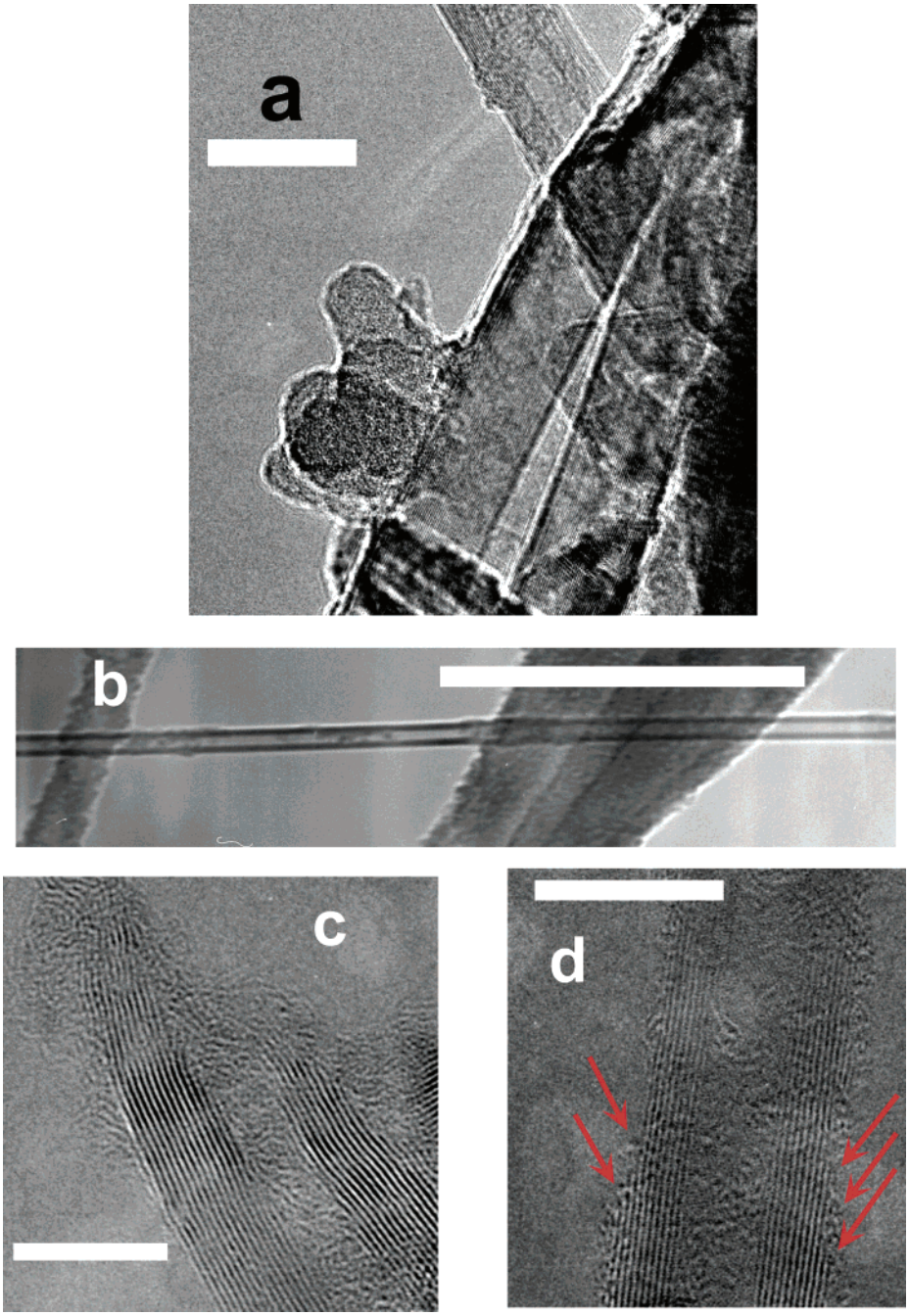


***Figure 1.*** (a) High-resolution TEM image of pristine, unprocessed multiwalled nanotubes. Scale bar represents 20 nm. (b) Low-resolution TEM image of a processed, "clean" tube. Scale bar represents 125 nm. (c) Open tip of an oxidized MWNT. (d) Serrated edges where the outer wall has been substantially etched away. Scale bars represent 7 and 8 nm, respectively, for these high-resolution images. Arrows point to areas on the MWNT where the outer wall has been etched away, leaving behind dangling oxygenated, functional groups.

**Electron Microscopy.** Samples for TEM and HRTEM were obtained by drying sample droplets from an ethanolic solution onto a 300 mesh Cu grid covered with a lacey carbon film. A Philips CM12 TEM, equipped with EDAX capabilities, was used at an accelerating voltage of 120 kV for low-resolution imaging. High-resolution images were obtained on a JEOL 2010F HRTEM, equipped with an Oxford INCA EDS system, at an accelerating voltage of 200 kV. SEM samples were drop dried onto Cu grids and held over a Be plate inside a homemade sample holder. Samples were imaged on a Leo 1550 field emission instrument using accelerating voltages of 2−10 kV at a 2 mm working distance.

**X-ray Photoelectron Spectroscopy.** The samples were attached to stainless steel holders using conductive double-sided tape and placed in the vacuum chamber of a model DS800 XPS surface analysis system (Kratos Analytical Plc, Manchester, United Kingdom). The chamber was evacuated to a base pressure of $\sim 5 \times 10^{-9}$ torr. A hemispherical energy analyzer was used for electron detection. XPS spectra were first collected using a Mg K$\alpha$ X-ray source at 80 eV pass energy and at 0.75 eV steps. High-resolution spectra were collected at a pass energy of 10 eV and in 0.1 eV steps.

**X-ray Diffraction.** Powder X-ray diffraction spectra were collected on a Scintag diffractometer, operating in the Bragg configuration using Cu K$\alpha$ ($\lambda = 1.54$ Å) radiation.

**Optical Spectroscopy.** UV-visible spectra were obtained at high resolution on a Thermospectronics UV1 using quartz cells with a 10-mm path length. UV-visible spectra were obtained for CdTe nano-

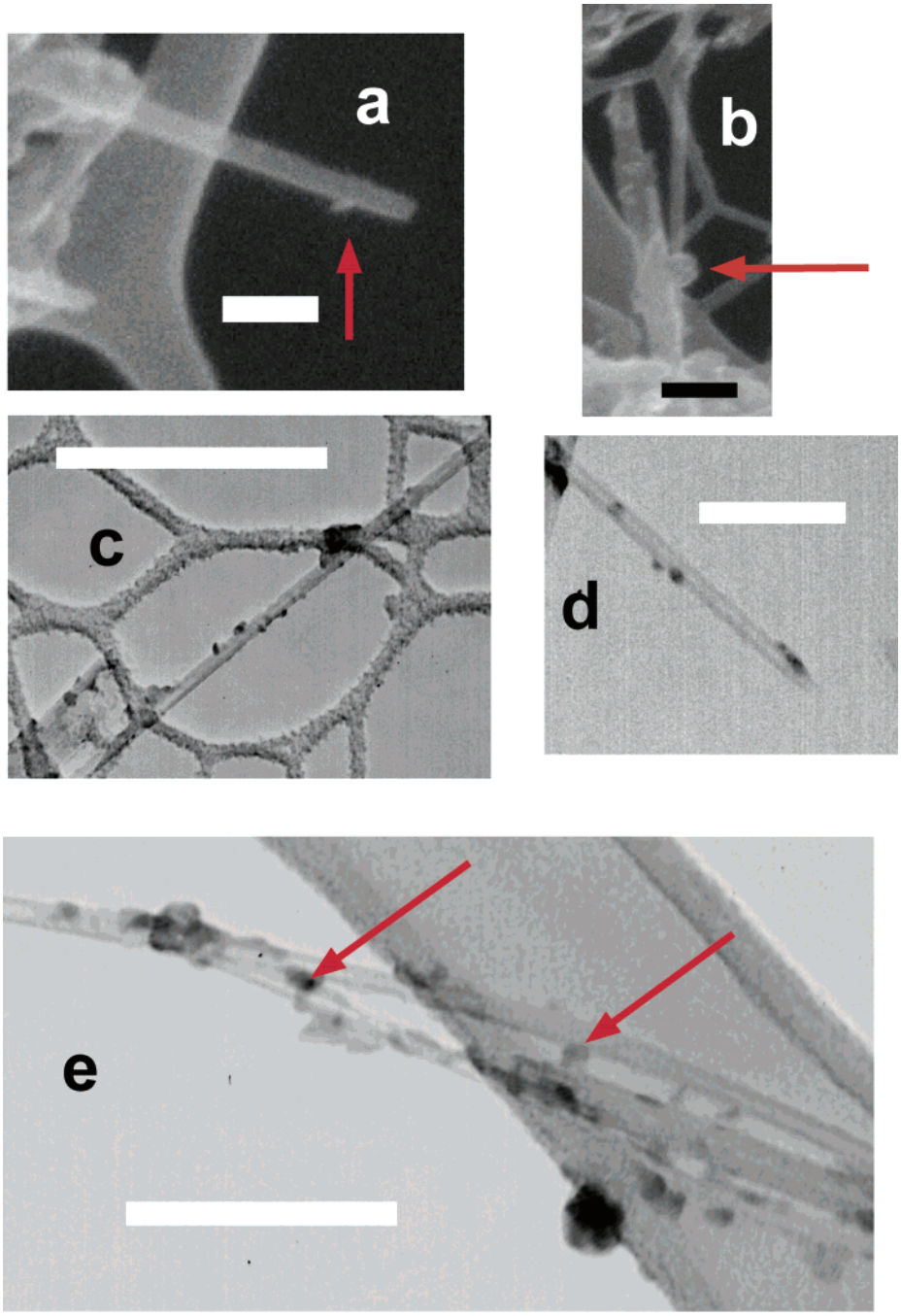


***Figure 2.*** (a) Scanning electron micrograph (SEM) of a particle grown near the tip of the tube. (b) SEM image of a nanocrystal-mediated junction with carbon nanotube bundles. Arrows point to CdTe. Scale bars for SEM images are 100 and 200 nm, respectively. Presence of CdTe was confirmed by EDS signals for Cd and Te. Parts c−e show transmission electron microscopy images. (c) Sidewall coverage of quantum dots on a MWNT bundle. (d) CdTe nanocrystals on nanotube sidewalls, with some near the tip edge. (e) Nanocrystal-mediated nanotube junctions indicated by arrows. Scale bars for TEM images are 180, 75, and 112 nm, respectively.

crystals, dissolved in toluene, and for the nanotube-nanocrystal heterostructure, dispersed by sonication in DMF. Infrared spectra were obtained, using a ThermoNicolet Nexus 670 using a ZnSe single reflectance ATR accessory. Samples for Raman spectroscopy were analyzed on a Jasco Ventuno micro-Raman instrument, with a 200 micron confocal aperture, at a diode laser excitation of 785 nm using a power of 10 mW.

## Results and Discussion

**Microscopy Characterization.** Figure 1 shows TEM images of our initial building blocks, namely purified and oxidized MWNTs (Figure 1b). Pristine, unoxidized tubes are shown in Figure 1a. The aggressive oxidation regime described can open the caps of the MWNTs (Figure 1c) as well as partially oxidize and remove some of the outer layers of the tubes (Figure 1d). This acid oxidation is able to etch away at the tube's outer walls and at defect sites. The clearly visible, serrated edges of the walls (Figure 1d) and the open ends (Figure 1c) of these processed tubes, observed in the HRTEM images, have dangling bonds and oxygenated functional groups, which are then able to act as ligands for the growth of CdTe nanocrystals. The presence of serrations in processed tubes stands in sharp contrast to the highly crystalline graphite lattice seen in the unpurified

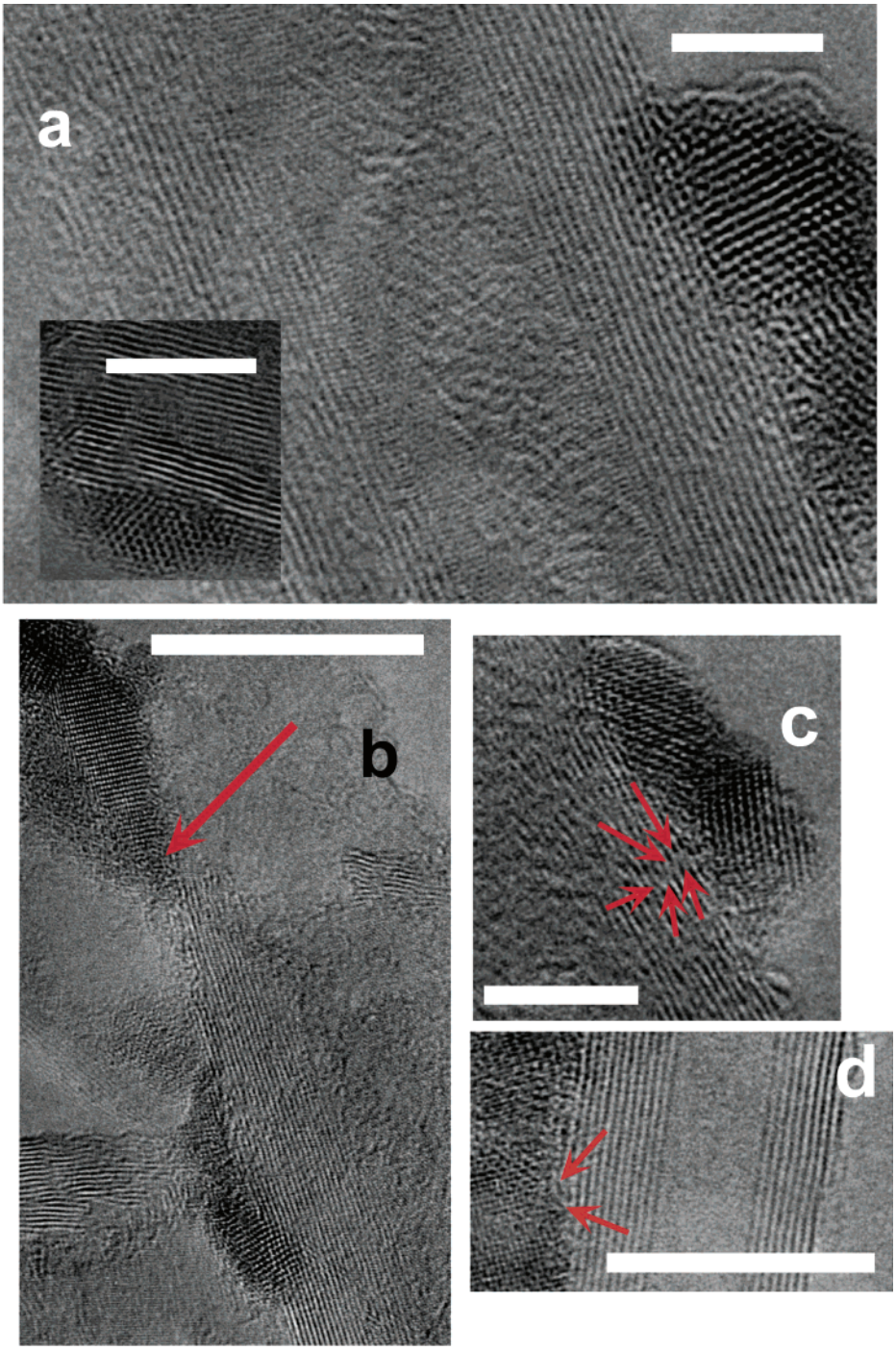


***Figure 3.*** (a) High-resolution TEM images of CdTe nanocrystals grown on a MWNT surface. Inset shows a different nanotube−nanocrystal composite. Scale bars are 5 nm in both cases. (b) An elongated CdTe nanocrystal grown at the opened tip of a MWNT. Arrow indicates site of attachment between the nanotube and nanocrystal. (c) CdTe nanocrystal grown at a defect site. Arrows circumscribe a defect site where acid has etched through a few layers of the external sidewall. (d) Quantum dots grown from the serrated edges and etched sidewalls of the MWNT. Arrows depict ends of the walls where the crystals likely have nucleated. Scale bars for high-resolution data in parts (b) through (d) are 20, 5, and 10 nm respectively.

MWNT sidewalls in Figure 1a. The absence of any extraneous catalyst particles in these purified tubes was confirmed by XPS and EDS analyses.

Figure 2 displays SEM and TEM images of CdTe−MWNT nanoheterostructures. Especially notable is the contrast between the "clean" tube image, seen in Figure 1b, and the functionalized heterostructure, visible in parts c and d of Figure 2. Parts a and d of Figure 2 show a relatively higher density of particles near the MWNT tip. Functionalization at these sites on the nanotube is expected to be more facile because of the expected abundance of oxygenated functional groups, which can nucleate the growth of nanocrystals. In fact, the high density of functional groups at these sites has been noted previously and is due to the curvature-induced increased reactivity at positions close to the tip.[38] After tip opening, acid etching can destroy most of the outermost walls of the MWNT close to the tip.[39] We and others have previously noted an analogous high density of nanocrystal attachment at nanotube ends through reactions mediated by

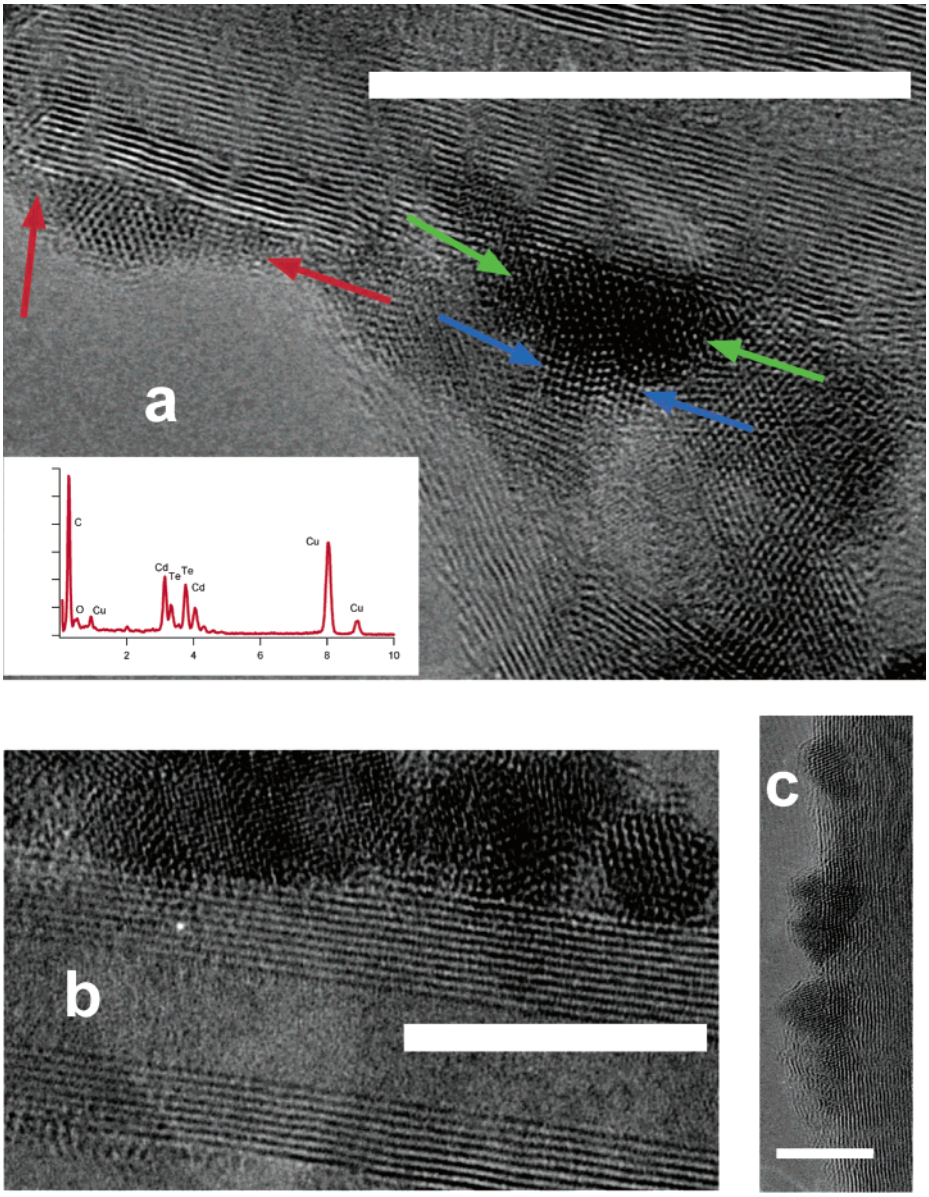


***Figure 4.*** (a) High-resolution TEM image of a junction with a nanocrystal in the middle of and attached to two nanotube bundles. Sets of arrows define irregularly shaped nanocrystals. Inset shows an EDS spectrum of the nanotube−nanocrystal heterostructure. Horizontal axis is energy in eV. (b) and (c) High-resolution TEM images demonstrate extensive sidewall coverage of in situ nanocrystals. Scale bars are 20, 10, and 10 nm respectively.

covalent, amidation chemistry.[28,29] However, because of our use of a more aggressive oxidation regime, we are not limited to derivatization simply at the ends of the tubes.[29] Figure 2, in fact, demonstrates significant tethering of nanocrystals to the MWNT sidewalls.

Parts b and e of Figure 2 demonstrate the versatility of the in situ growth technique in the construction of nanoscale junctions, composed of nanotubes, adjoined by interceding nanocrystals. In contrast, covalent attachment, mediated by carbodiimide, typically yields only isolated, randomized nanotube−nanocrystal heterostructures.[28,29] The expected presence of Cd, Te, and P, originating as a secondary ligand from TDPA, in our heterostructures was confirmed by EDS analysis.

High-resolution TEM images show well-defined lattice fringes for CdTe nanocrystals, grown on the tube walls as seen in Figure 3a, forming clear interfaces. The crystals are predominantly wurtzite in structure, though at least some of these crystals appear to be of the cubic zinc blende morphology. The HRTEM images in Figure 3 lend useful insight into possible mechanisms of CdTe nanocrystal growth at the tube ends and surface edges, where there is preferential attachment of these crystals. Figure 3b shows an irregularly shaped CdTe crystal, grown at the open tip edge of a MWNT, all of which are lying on top of a carbon film. Figure 3c illustrates nanocrystals grown from a defect site at an apparent discontinuity on the nanotube sidewall. The acid seems to have etched through several layers of the sidewall. Another common motif is the presence of nanocrystals attached to the outermost, exposed edges of the tubes, as observed in Figure 3d as well as in the inset to Figure 3a. Hence, these areas, including the tips of the MWNTs, are

(38) Ajayan, P. M.; Ebbesen, T. W.; Ichihashi, T.; Iijima, S.; Tanigaki, K.; Hiura, H. *Nature* **1993**, *361*, 333.
(39) Yao, N.; Lordi, V.; Ma, S. X. C.; Dujardin, E.; Krishnan, A.; Treacy, M. M. J.; Ebbesen, T. W. *J. Mater. Res.* **1998**, *13*, 2432.

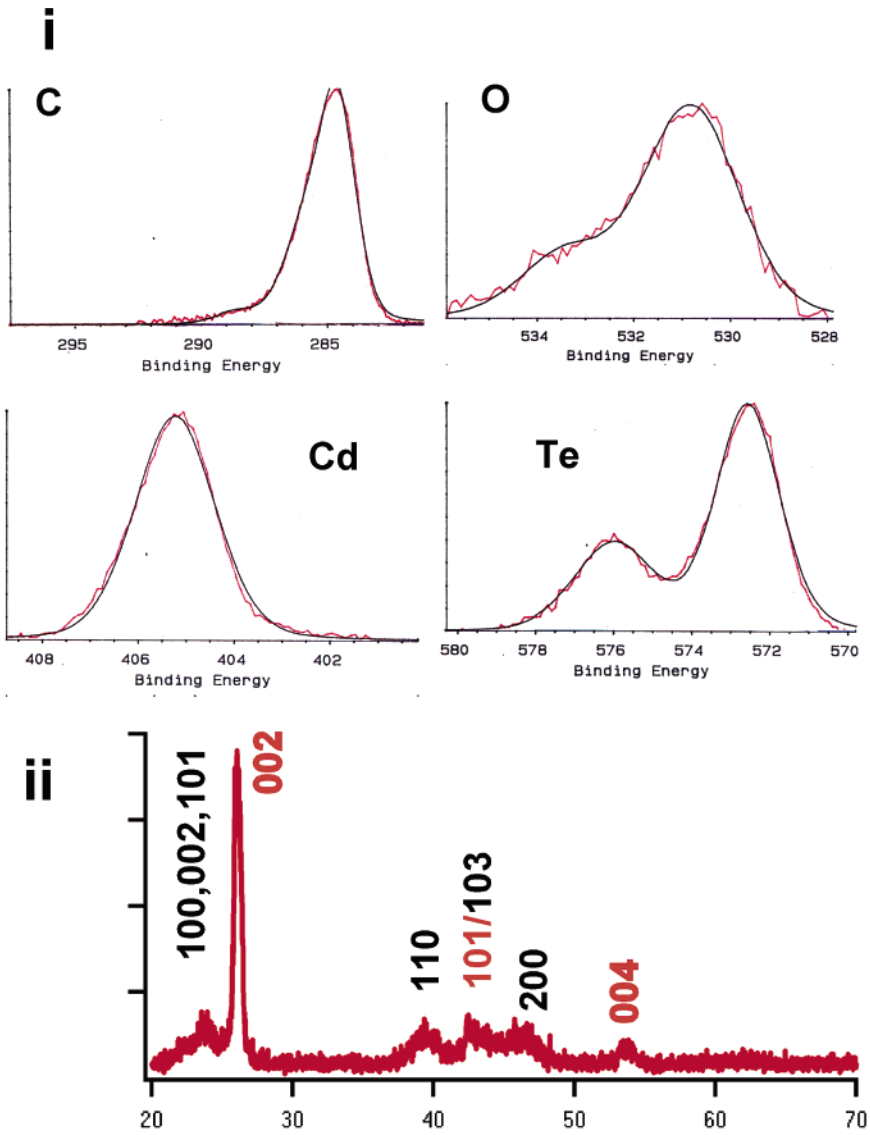


***Figure 5.*** (i) High-resolution XPS spectra (clockwise from top left) for C 1s, O 1s, Te $3d_{5/2}$, and Cd $3d_{5/2}$ signals. Bottom axis represents binding energy (in eV). Vertical axis is intensity in arbitrary units. (ii) X-ray diffraction pattern for CdTe−MWNT heterostructure. Vertical axis is intensity in arbitrary units. Horizontal axis is $2\theta$. Peaks indexed in black correspond to wurtzite CdTe, whereas those labeled in red are associated with MWNTs. The presence of zinc blende-stacking faults, as well as some zinc blende crystals, is also likely. However, these zinc blende peaks are very near to those of wurtzite and, hence, may overlap.

particularly susceptible to oxidative attack, are richly populated with oxygenated functional groups, and are thereby able to act as nucleation sites for the growth of nanocrystals.

The elongated shape of the nanocrystal, evident in Figure 3b, can be explained by a diffusion-limited growth process.[40] The MWNT limits access to one face of the growing crystallite, and the incoming monomer flux adds preferentially onto the other free end, thereby inducing a pseudo-one-dimensional growth for the crystal. This apparent control over resulting nanocrystal shape can be attributed to a steric effect due to the bulky nanotube ligand, a phenomenon which has also been noted in molecular coordination complexes of nanotubes.[32,33] In other words, the nanotube influences directional diffusion of the monomer.

Parts b and c of Figure 4 show a high density of nanocrystals grown on MWNT sidewalls. Whereas "free" nanocrystals, washed away during sample workup, are relatively monodisperse in size and shape (quasi-spherical, 5 nm) because they originate predominantly from previously studied growth processes involving primarily cadmium−phosphonic acid precur-

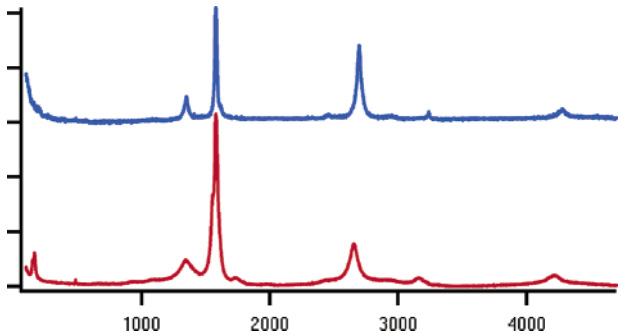


***Figure 6.*** Raman spectra. Horizontal axis is in wavenumbers. Vertical axis is intensity in arbitrary units. Top spectrum (in blue) is associated with oxidized and purified MWNTs used as a precursor to the heterostructure formation. Lower figure (in red) is a Raman spectrum of the CdTe−MWNT heterostructure product.

(40) Peng, Z. A.; Peng, X. *J. Am. Chem. Soc.* **2001**, *123*, 1389.

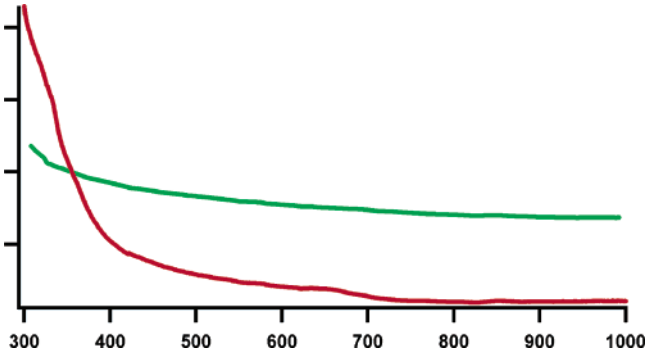


***Figure 7.*** Electronic spectra. Horizontal axis represents wavelength (in nm). Vertical axis is intensity in arbitrary units. Spectrum (lower, in red) is taken of CdTe washings. Spectrum (upper, in green) is associated with the CdTe−MWNT heterostructure.

sors,[37] nanocrystals grown on the surfaces of the tubes are strongly affected by the nanotube ligand. The large variation observed in the shape and size of these latter nanocrystals likely arises from factors such as functional group density at a particular site, the geometry of the site (the spatial location on the tube and the ability of MWNTs to control diffusion of the monomer flux), and the physical distance separating functional groups on the same tube or on adjacent tubes. The length of the long axis of these in situ-grown nanocrystals ranges from 1 to 9 nm, and the aspect ratio varies from 1 to 5. The spacing between tubes would be responsible for the junctions observed in parts b and e of Figure 2 and at high resolution in Figure 4a.

From all of these microscopy results, it is evident that nanotube−nanocrystal heterostructure formation is chemically mediated. Oxidized nanotubes essentially act as a template for the in situ growth of quantum dots, effectively controlling the shape and size of the nanocrystals thereby formed. In successive control experiments, quantum dot growth experiments have been performed with pristine, raw, and mildly oxidized tubes. We have noted that the extent of functionalization of nanotubes with nanocrystals correlates, in large measure, with the degree of tube oxidation. In particular, the aggressive oxidation regime described here enables a high surface coverage of quantum dots on the ends as well as at numerous sites on the sidewalls. It should be noted that few, if any, nanocrystals were observed coordinated to pristine, unoxidized nanotubes. All of the results presented here correlate with highly oxidized MWNTs containing ∼5−6 atomic % oxygen content as determined by XPS. In contrast, mildly oxidized MWNTs, with oxygen contents of ∼1−2 atomic %, showed very sparse coverage of coordinated nanocrystals.

**Additional Structural Characterization.** Further confirmation for heterostructure formation comes from analysis of XRD and XPS measurements. XRD indicates that the predominant crystal structure is wurtzite, although some contribution from zinc blende-stacking faults as well as from zinc blende nanoparticles is also expected. Associated peaks have been indexed (Figure 5ii). The peaks are broadened with respect to analogous bulk data because of the finite size of the particles. XPS measurements (Figure 5i) also establish the formation of CdTe on the nanotube surface. The $C_{1s}$ high-resolution peak shows conspicuous asymmetry, including a pronounced contribution from the high binding energy side, corresponding to the presence of carboxylic acids and carboxylate-like surface structures. The Cd $3d_{5/2}$ peak, shown at high resolution, can be fit perfectly to

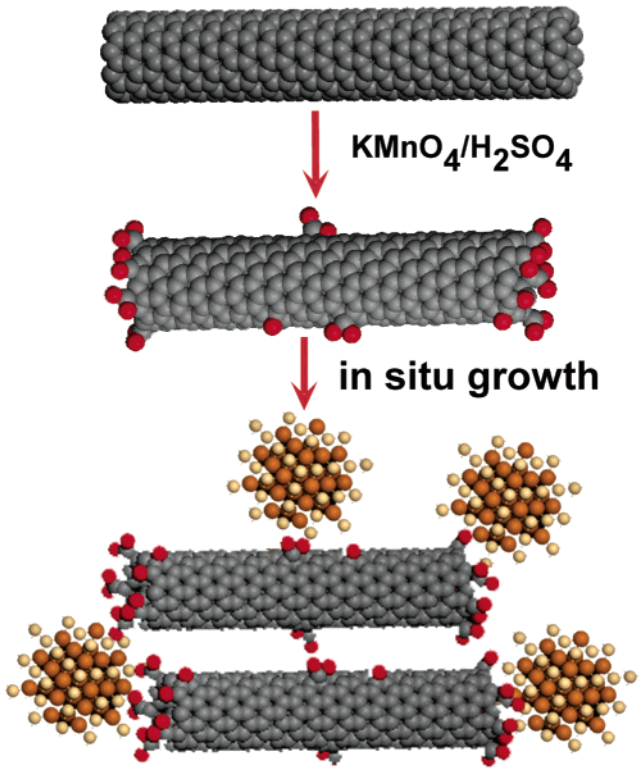


***Figure 8.*** Schematic illustrating various steps in the growth of the nanotube−nanocrystal heterostructure. Pristine nanotubes are oxidized to generate functional groups at the nanotube ends and at a few defect sites. CdTe nanocrystals are then grown in situ by coordination of Cd and injection of a Te solution as described in the Experimental Section. TDPA ligands to the CdTe are omitted for the sake of clarity. Probable structures for junctions between multiple tubes are also depicted.

CdTe with a binding energy of Cd at 405.22 eV. The $TeO_3$ peaks, ascribed to Te $3d_{5/2}$, attest to formation of species due to inadequate surface passivation of the CdTe. This is expected, since the number of nanotubes that can coordinate to the nanocrystal surface is physically constrained by the intrinsic bulk of the tube. Thus, under ambient conditions and upon prolonged exposure to air, some decomposition will take place, as with most quantum dots, because of the formation of surface species such as $TeO_3$. This process is further hastened at higher temperatures. Heating can also remove the carboxyl groups on the MWNTs themselves, although not completely until approximately 350 °C. The intrinsic structures of nanotubes and of the resulting nanocrystals, however, are expected to remain intact to such temperatures.

Raman scattering measurements (Figure 6) are also consistent with the formation of a confined CdTe cluster. Raman spectra for the heterostructure at 785 nm excitation show an expected longitudinal optic (LO)-type band with a peak at 166 $cm^{-1}$, which is missing from the Raman spectra of the precursor MWNTs used in the study. The downshift and broadening of this mode from the bulk peak, occurring at 170 $cm^{-1}$, has been previously observed in Raman scattering studies on CdTe clusters.[41] Raman spectra of the precursor sample and the MWNT-CdTe heterostructure show bands characteristic of nanotubes, namely the high-frequency G modes[42] near ∼1590

(41) Rolo, A. G.; Vasilevskiy, M. I.; Gaponik, N. P.; Rogach, A. L.; Gomes, M. J. M. *Phys. Status Solidi B* **2002**, *229*, 433.

$cm^{-1}$ and a weaker disorder mode peak at 1290−1320 $cm^{-1}$ (D band).

The electronic spectrum (Figure 7) of the nanotube-adduct is featureless, and no CdTe exciton can be resolved. This is likely due to both the large background absorbance of the nanotube and the large variation in size and shape of the nanocrystals attached to the MWNT surface, as described previously. The spectra of the toluene washings also show a lower degree of monodispersity for these nanocrystals relative to those quasi-spherical nanocrystals (∼5 nm), grown without nanotubes as ligands. Thus, MWNTs likely affect the growth of a portion of the washed-away crystals. We explain this postulate as related to the fact that many from this class of nanocrystallites likely come loose from the nanotubes at various stages of their growth process, thereby accounting for the larger heterogeneity in quantum dot size observed. This is a further indication that functionalized nanotubes provide a spatially constraining template that favors one-dimensional growth[40] and, hence, anisotropic quantum dot formation.

## Conclusions

This current work demonstrates in situ mineralization of CdTe on MWNT surfaces. Use of coordination chemistry is hence shown as a viable route to the synthesis of nanotube-based heterostructures (Figure 8). The resulting nanotube−nanocrystal heterostructures have been extensively characterized, and the nanocrystals appear to be in the quantum-confined regime. The extent of functionalization as well as the sites of functionalization are controlled by the density and abundance of oxygenated functional groups on the MWNT surface. It has proven to be far more challenging to generate a high enough density of functional groups, using conventional oxidative methods, on single-walled carbon nanotubes in order to grow a large enough number and density of nanocrystals on those tubes, without seriously compromising tubular structural and electronic integrity. Increased control and refinement of oxidative protocols[43] are likely to result in more sophisticated examples of the hierarchical architectures presented here.

Our results will have relevance for the design of future molecular electronic and photovoltaic devices with unique nanoscale electronic properties. The method we propose also addresses the generation of tailorable interconnects with predictable features. Nanotube−nanocrystal devices present an interesting illustration of the idea of bottom-up assembly using nanoscale building blocks. Future research will focus on charge transport through these nanoscale junctions, growing nanocrystals across junctions of aligned tubes, as well as developing thin films of these composite materials.

**Acknowledgment.** We acknowledge support of this work through startup funds provided by the State University of New York at Stony Brook as well as Brookhaven National Laboratory. Acknowledgment is also made to the donors of the Petroleum Research Fund, administered by the American Chemical Society, for support of this research. S.S.W. thanks 3M for a nontenured faculty award. We also thank Professor Jianyu Huang (Department of Physics, Boston College) and Dr. James Quinn (Materials Science, SUNY at Stony Brook) for their help with HRTEM and SEM/TEM analyses, respectively. The assistance of Craig Silverman (Jasco) with Raman analyses has been appreciated. Drew Hirt (Materials Research Laboratories, Inc.) is acknowledged for his work with the XPS results.

**Supporting Information Available:** Infrared spectrum of oxidized multiwalled nanotubes (PDF). This material is available free of charge via the Internet at http://pubs.acs.org.

JA035980C

(42) Rao, A. M.; Richter, E.; Bandow, S.; Chase, B.; Eklund, P. C.; Williams, K. A.; Fang, S.; Subbaswamy, K. R.; Menon, M.; Thess, A.; Smalley, R. E.; Dresselhaus, G.; Dresselhaus, M. S. *Science* **1997**, *275*, 187.

(43) Banerjee, S.; Wong, S. S. *J. Phys. Chem. B* **2002**, *106*, 12144.